

Molecular insights into the effect of alkanediols on FUS liquid-liquid phase separation

Theodora Myrto Perdikari¹, Anastasia C. Murthy^{2,3}, Nicolas L. Fawzi^{4*}

¹Center for Biomedical Engineering, Brown University, Providence, RI, USA

²Molecular Biology, Cell Biology & Biochemistry Graduate Program, Brown University, Providence, RI, USA

³Department of Early Discovery Biochemistry, Genentech Inc., South San Francisco, CA, USA

⁴Department of Molecular Biology, Cell Biology & Biochemistry and Robert J. and Nancy D. Carney Institute for Brain Science, Brown University, Providence, RI, USA

*Correspondence: nicolas_fawzi@brown.edu

Abstract

Numerous cell biology studies have used high concentrations of 1,6-hexanediol to dissolve membraneless organelles and disordered protein biomolecular condensates. Yet, little is known about how alkanediols effect liquid-liquid phase separation (LLPS), and why certain alkanediol isomers are more effective. Here, we evaluate the effect of various alkanediols on the archetypal phase separating protein FUS. Low-complexity domain and full-length FUS LLPS is decreased varyingly, while LLPS of FUS RGG-RNA condensates is even enhanced by some alkanediols. NMR experiments show that all diols act similarly, correlating atomistic changes with LLPS-preventing effects. Furthermore, we find no evidence for specific residue interactions – the largest perturbations are seen at backbone and glutamine side-chain hydrogen bonding sites, not hydrophobic/aromatic residues. Furthermore, 1,6 hexanediol favors formation of protein-solvent hydrogen bonds and increases FUS local motions. These findings show how alkanediols affect water-disordered protein interactions, underscoring the difficulty in using alkanediol-derivatives to target dissolution of specific membraneless organelles.

Introduction

Cellular biochemistry is spatiotemporally tuned by intracellular compartments which are termed biomolecular condensates because, despite lacking a phospholipid bilayer, they condense high concentrations of heterogeneous biomolecules through a process called liquid-liquid phase separation (LLPS)(Banani *et al*, 2017). The formation, dissolution and localization of membraneless puncta is controlled by a plethora of factors such as presence of RNA(Roden & Gladfelter, 2021) and post translational modifications to proteins that often contain intrinsically disordered regions (IDRs)(Snead & Gladfelter, 2019). Moreover, the formation or stability of some cytoplasmic and nucleoplasmic condensates such as stress granules (SGs)(Wolozin & Ivanov, 2019) and the nuclear pore complex (NPC) are sensitive to the cellular uptake of some small organic aliphatic alcohols(Shulga & Goldfarb, 2003; Kroschwald *et al*, 2015a; Wheeler *et al*, 2016). Specifically, alcohols that were first shown to interfere with nuclear pore function(Jäggi *et al*, 2003), have been employed to assess the reversibility of liquid nuclear and cytoplasmic puncta(Kroschwald *et al*, 2015). For example, 1-6 hexanediol, 1-2 hexanediol and 1-5 pentanediol are capable of dissolving nucleopores(Patel *et al*, 2007), RNA granules and cytoplasmic granules(Tulpule *et al*, 2021) by putatively disrupting weak hydrophobic interactions. Yet, in these same studies, the 2,5 isomer of hexanediol does not have similar levels of activity. 1,6 hexanediol is often assumed to alter hydrophobic interactions, possibly by specific contacts with proteins, yet disordered protein LLPS is often described as being mediated predominantly by π contacts, especially tyrosine and arginine (Wang *et al*, 2018). In addition, these aliphatic alcohols appear to specifically disassembly liquid-like assemblies, not protein aggregates. In yeast, when 1-6 hexanediol was used in tandem with compounds that increase cell permeability like digitonin, P granules dissolved but stress granules with a more solid-like character remained intact(Kroschwald *et al*, 2017), showing that alkanediols do not act as simple denaturants. In mammalian cells, 1-6 hexanediol was used to probe the liquidity of stress granules but prolonged exposure is cytotoxic and generated abnormal cell

morphologies(Wheeler *et al*, 2016). Additionally, recent studies have also shown that 1,6 hexanediol can condense chromatin, suggesting protein-nucleic acids assemblies may behave differently in alkanediols than phase separation mediated by disordered proteins. Although these studies provide compelling evidence that small organic alcohols can be used to assess the physical properties of *in vitro* reconstituted droplets and cellular condensates, the details of how the molecular interactions underlying liquid-like assembly are perturbed in the presence of these molecules remain unclear.

FUS (Fused in Sarcoma), is an extensively characterized phase-separating DNA/RNA-binding protein that has been in the spotlight for its disease-causing mutations(Patel *et al*, 2015) and its LLPS-mediating interactions with nucleic acids(Loughlin *et al*, 2019; Daigle *et al*, 2013), nucleic acid-mimic biopolymers(Altmeyer *et al*, 2015), and transcription factors(Owen *et al*, 2021). FUS LLPS is also modulated by phosphorylation (Monahan *et al*, 2017) and arginine methylation (Hofweber *et al*, 2018). Under physiological conditions, FUS can shuttle between the nucleus and the cytoplasm and forms interactions with other proteins through its serine-glutamine-tyrosine-glycine (SQYG) rich N-terminal disordered region, arginine-glycine (RGG) motifs (Chong *et al*, 2018) and globular nucleic acid binding domains(Deng *et al*, 2014). Because aberrant function of membraneless puncta containing FUS has been associated with pathology, particularly in neurodegenerative disease and cancer (Ryan & Fawzi, 2019; Alberti & Dormann, 2019; Boija *et al*, 2021), focus has turned towards targeting proteins undergoing LLPS with small drug-like molecules (Klein *et al*, 2020; Babinchak *et al*, 2020; Schmidt *et al*, 2021). Although the molecular homotypic and heterotypic interactions holding together the condensed phase of FUS such as hydrophobic, π^2/π contacts, and hydrogen bonds have been studied in detail (Murthy *et al*, 2019)(Murthy *et al*, 2021), little is known on the atomic level about how non-covalent interactions with aliphatic alcohols perturb the phase-behavior of FUS. Although hydrophobic interactions are thought to be disrupted and particular alkanediol-protein interaction geometries have been hypothesized to be important for this action(Kato & McKnight,

2018), it remains unclear why certain alkanediols are effective in altering LLPS while others including isomers of the same compound are not.

To fill this gap, here we use microscopy, solution-state NMR, and biochemical assays to unravel the molecular-level details of FUS interactions with condensate-modifying molecules. We test the effect of alkanediols of different length, configuration, and hydrophobicity on the phase-separation, molecular structure, and motions of FUS SYGQ LC domain. In particular, we seek to answer the outstanding question if specific molecular interactions (e.g. with particular amino acids or regions) are formed between alkanediols and the protein. This work provides a systematic framework to evaluate the effect of LLPS-modulating molecules and potentially inform the design of therapeutics against intrinsically disordered protein targets that minimize aberrant phase transitions while maintaining physiological biomolecular condensation.

Results

Effect of alkanediols on FUS SYGQ LC LLPS and chemical environment.

Aliphatic alcohols such as 1,6-hexanediol (1,6-HD), 2,5-hexanediol (2,5-HD), 1,4-butanediol (1,4-BD) and 1,5-pentanediol (1,5-PD) have been extensively used as FUS hydrogel melting (Lin *et al*, 2016) and phase separation prevention (Berkeley *et al*, 2021) (Li *et al*, 2021), agents. We sought to determine how a series of different alkanediols, including also 1,2-hexanediol (1,2-HD) and 1,2-cyclohexanediol (1,2-CHD), alters the capacity of the purified isolated low-complexity (LC) domain (residues 1-163) of FUS to form liquid droplets *in vitro*. Using differential interference contrast (DIC) microscopy, we found that the liquid-like droplets were dissolved completely in 5% of 1,2-CHD, 1,2-HD, 1,6-HD, or 1,5-PD but persisted in 5% 1,4-BD and 5% 2,5-HD with the latter diol being the least efficient among the series of hexanediol isomers being tested (**Figure 1A**). The same behavior is seen at later time points (**SI Figure 1**). Next, we quantified the effect on FUS LC LLPS of the same alkanediols by inducing phase separation with inclusion of salt and then measuring the amount of FUS LC remaining in

the supernatant after centrifugation to sediment FUS LC droplets (**Figure 1B**). Compared with the rest of hexanediol series, both 2.5% and 5% 2,5-HD resulted in lower concentration of protein remaining in the dispersed phase and higher turbidity (**Figure 1C**) suggesting that this isomer of hexanediol is the least efficient disrupting the condensed phase. Alkanediols of shorter carbon chain length such as butanediol and pentanediol reduced the extent of phase separation but did so less than hexanediols with hydroxyl groups at positions 1,6 and 1,2. Next, we sought to test if the higher effectiveness of some alkanediols could be attributed to particular contacts with FUS. NMR chemical shift measurements are uniquely sensitive, residue-by-residue probes of the structure and interactions at every site in a protein. We acquired ^1H - ^{15}N HSQC spectra of FUS SYQC LC domain in the presence of either 2.5% or 5% of a different aliphatic alcohol each time and we mapped the chemical shift perturbations to identify locations with changes in chemical environment (e.g. conformational change or interaction) (**SI Figure 2**). Although we analyze the sequence specific spectral changes below (see below), here we show that the chemical shift perturbations of each diol are highly correlated with those for 1,6-hexanediol, though 1,6-hexanediol and 1,2-hexanediol have the largest magnitude at 5% (**Figure 1D**). In other words, the sequence-specific effects are largely the same for all diols tested. The observation that the series of alkanediols show a quantitative gradient of effects on LLPS and chemical environment with qualitative similarity suggest that all alkanediols have similar mechanisms of action. Hence, we do not find evidence for specific interactions caused by particular alkanediols or isomers. Furthermore, the magnitude of the chemical shift perturbations is strongly correlated with the activity of these molecules in the phase separation assay (**Figure 1E**) as shown by Pearson's correlation coefficient (PCC = 0.85). Hence, the changes in residue-by-residue perturbation of the chemical environment are strongly correlated with the mechanism of action. Conversely, the effect on LLPS is not correlated with the predicted water solubility (logP) of each diol (**SI Figure 1B,C**) (Cheng *et al*, 2007). Molecules with similar predicted partition coefficient such as 1,2-hexanediol (which also has significantly

lower experimentally-determined solubility than 1,6 hexanediol) and 2,5-hexanediol show different impacts on LLPS. Together, the data suggest that alkanediols of varying ability to disrupt LLPS have qualitatively similar impacts on the molecular environment of FUS LC but are distinguished by the magnitude of these effects.

FUS RGG3-RNA rich droplets are insensitive to the treatment with alkanediols.

Inspired by recent studies on the effect of hexanediol in the organization of chromatin(Shi *et al*, 2021; Liu *et al*, 2021; Ulianov *et al*, 2021) and RNA granules(Fuller *et al*, 2020) as well as by reports on the action of chemotherapeutics on nucleolar proteins and ribosomal RNA (rRNA) synthesis(Sutton & DeRose, 2021), we studied the capacity of condensate-modifying agents to inhibit phase separation of FUS in the presence of RNA as a model for the types of protein-RNA interactions that contribute to biomolecular condensates formed in cells. As previously(Burke *et al*, 2015; Monahan *et al*, 2017), we imaged FUS full-length after the addition of TEV protease to cleave the solubilizing MBP-tag (**Figure 2A**). As expected, 1,6-hexanediol disrupts phase separation of FUS (**Figure 2A**). As we showed previously, addition of RNA (here we use polyadenylic acid (polyA) RNA) enhances phase separation. Importantly, we find that phase separation is modestly decreased but still present even with addition of aliphatic alcohols (**Figure 2A**) as seen by high turbidity values (**Figure 2B**). Hence, 1,6-hexanediol is not able to fully dissolve FUS full-length condensates with RNA, suggesting that phase separation of RNA with other domains of FUS including RGG domains may not be perturbed by hexanediol. To further test this hypothesis and exclude the possibility that the cleaved MBP tag or TEV protease interferes with the ability of hexanediol to dissolve these condensates, we used FUS RGG3 (purified apart from an MBP-tag) that phase separates readily upon addition of RNA. Like FUS full-length, RGG3-RNA condensates at these conditions were still observed in the presence of all alkanediols (**Figure 2C**) and phase separation is not markedly decreased (**Figure 2D**). Interestingly, 5% 1,2-cyclohexanediol even appears to

enhance phase separation of RGG3 and RNA (**Figure 2D**). Similarly, increased turbidity was also observed in the presence of RNA and some alkanediols (**Figure 2E**). Imaging the RGG3-RNA condensates over time showed that droplets remained spherical (**SI Figure 3**). Together these data suggest that while alkanediols readily disrupt SYGQ-rich LC domain phase separation, they are not capable of disrupting electrostatic interactions that are responsible for RNA-protein co-phase separation.

1,6-hexanediol does not substantially alter the local disordered structure of FUS SYGQ LC but enhances reorientational molecular motion.

To obtain a more detailed insight into the interactions of this compound with FUS SYGQ LC, we acquired a ^1H - ^{15}N heteronuclear single quantum coherence (HSQC) spectrum in the presence of 5% 1,6-hexanediol (**Figure 3A**). We quantified the chemical shift perturbations between the control and 1,6-hexanediol conditions and observed weak non-specific interactions throughout FUS SYGQ LC domain (**Figure 3B**). To decipher the contribution of each assigned residue type in the detected differences, we binned the chemical shift perturbations and we found that specific amino acids show distinct chemical shift difference in the presence of 5% 1,6-hexanediol (**Figures 3C, D**). Threonine and alanine show the largest average perturbation in both ^1H and ^{15}N chemical shifts, though the distribution of shifts for each residue type is large, especially for the most common residue types (serine, glycine, glutamine, and tyrosine). To examine if 1,6-hexanediol causes chemical shift differences in a sequence-specific manner, we acquired a ^1H - ^{15}N HSQC spectrum of FUS RGG3, a shorter fragment with different amino acid composition comprised mostly by arginine-glycine-glycine motifs. We observed, somewhat smaller magnitude of chemical shift perturbation (**SI Figure 4**) though a similarly large distribution of shifts for glycine, suggesting that 1,6-hexanediol similarly influences the chemical environment of highly distinct sequences. Hence, the chemical environment changes caused by

1,6-hexanediol are not specific to tyrosine-rich sequences, though the larger magnitude of the differences for FUS SYGQ LC may be due to disruption of tyrosine contacts (Martin *et al*, 2020).

Next, we examined the changes in local molecular motions of FUS SYQC LC due to 1,6-hexanediol by measuring the ^{15}N spin relaxation parameters (R_1 , R_2 , hetNOE) at each backbone amide position (**Figure 3E**). These experiments are sensitive to reorientational motions of the amide (NH) bond vector on the ps to ns timescales (Palmer *et al*, 2001). Decreased R_2 and elevated R_1 values in the presence of hexanediol suggest faster local reorientational tumbling motions whereas the magnitude of the hetNOE (i.e. below 0.5) is consistent with disorder across the domain and confirms that 1,6-hexanediol does not cause significant structural rearrangements of the isolated LC domain. Interestingly, similar decrease of ^{15}N R_2 is observed by introducing phosphomimetic serine-to-glutamate low complexity domain substitutions, FUS SYGQ LC 12E, which also prevents phase separation (Monahan *et al*, 2017). Hence, the elevated R_2 values likely report on dynamic interactions leading to phase separation (Martin *et al*, 2020) that are suppressed by charged residue substitution (e.g. FUS SYGQ LC 12E) or, as shown here, changes in the solvent environment (e.g. 1,6-hexanediol).

1,6-hexanediol induces larger FUS SYGQ LC NMR-detected perturbations at backbone carbonyl positions than the aliphatic side chains and aromatic sidechain positions.

Although the observed chemical shift changes in the presence of alkanediols are correlated with phase separation (**Figure 1**), the ^1H ^{15}N NMR data do not conclusively show if 1,6-hexanediol makes specific contacts that mediate its action or if it primarily alters the solvent environment. This is in part due to the limitation in inferring interactions by observing only the ^1H and ^{15}N amide positions. We next sought to determine if particular side chain types or other backbone regions show significant chemical shift perturbations. Because hexanediol is said to

affect hydrophobic interactions, we also probed the role of hydrophobic residue side chains by testing the hypothesis that some hydrophobic residue types would show larger side chain chemical shift differences than other side chains and backbone positions. To that end, we measured ^{13}C and ^1H chemical shift differences (**Figure 4**) for backbone (**Figure 4A**) and side chain carbon positions (**Figure 4B**). Both aliphatic and aromatic ^1H ^{13}C correlation spectra are nearly unperturbed by addition of 1,6-hexanediol (**Figure 4B**) and hence chemical shift differences are small (**Figure 4E,F**) and similar for side chain and main chain (i.e. α carbon positions). Despite the established importance of tyrosine in phase separation of FUS SYGQ LC (Murthy *et al*, 2019, 2021; Wang *et al*, 2018) and the intrachain contacts that tyrosine mediates in phase separating IDRs (Martin *et al*, 2020), the shifts for tyrosine aromatic positions are small and similar to side chain positions in other residue types. To compare the magnitude of these shifts to those observed on the backbone, we also measured chemical shift perturbations for carbonyl (^{13}CO) backbone positions (**Figure 4C,D**). These carbonyl positions are also potentially interesting as they are hydrogen bond acceptor sites and hexanediols are hydrogen bond donors. We performed a triple resonance HNCO experiments, correlating the amide ^1H and ^{15}N chemical shifts with the ^{13}C chemical shift of the preceding amino acid (Kay *et al*, 1990). Using sequential connectivity information from the previously assigned sequence of FUS LC (Burke *et al*, 2015), we obtained the ^{13}C chemical shift of the carbonyl resonance (CO) in the presence and absence of 5% 1,6-hexanediol (**Figure 4A**). These shifts are modest and not markedly correlated with the backbone ^{15}N perturbations (**SI Figure 5**). Classifying the CO chemical shift difference by residue type (**Figure 4D**) shows that polar residues such as serines, threonines, glutamines but also glycines show a wide range of chemical shifts. Surprisingly, many of the backbone ^{13}CO chemical shifts are larger than the ^{13}C aromatic (i.e. tyrosine) and aliphatic sidechain shift perturbations. Furthermore, the side chain ^{13}CO resonances (observed in the HNCO as a correlation with the minor population of side chain NH_2 where one hydrogen is replaced by deuterium due to exchange with the $^2\text{H}_2\text{O}$ lock solvent) are shifted ~ 0.07 ppm

(Figure 4A, inset), as large as the largest backbone ^{13}C shift (**Figure 4C**) and significantly larger than all other ^{13}C shifts. This large shift for glutamine side chain is unique given that the ^{15}N side chain of glutamine is shifted less (~ 0.04 ppm) (**Figure 3F**) than the largest backbone ^{15}N NH_2 (~ 0.20 ppm). Although complex details of structure and bonding contribute to chemical shift magnitude, the largest shift perturbations for ^{13}C positions are not at hydrophobic sites and instead at carbonyl positions, including the sidechain carbonyl of the 37 glutamine residues. Taken together, these data suggest that interactions between 1,6-hexanediol and FUS LC are relatively weak and non-specific, and there are not clear residue positions with largest effects (e.g. aromatic side chains). Furthermore, given that the largest differences are observed for backbone and sidechain positions that form hydrogen bonds, these results suggest that alkanediols alter the solvation of FUS LC and may disrupt hydrophobic interactions and hydrogen bonding.

1,6-hexanediol modestly enhances water solvation profile of FUS SYQC LC

Given that chemical shift perturbations in the presence of 1,6-hexanediol did not show specific residue interaction sites but rather indicated possible alteration of hydrogen bonding in FUS LC and changes in solvation, we probed if position-specific changes in hydrogen bonding in FUS LC could be revealed by measuring residue specific temperature coefficients (Baxter & Williamson, 1997; Cierpicki & Otlewski, 2001; Cierpicki *et al*, 2002). Amide ^1H resonance positions as a function of temperature are a sensitive indicator of hydrogen bonding status. In general, temperature coefficients more negative than -4.5 ppb/K are observed for non-hydrogen bonded amides (e.g. amides open to solvent interaction, not engaged in protein-protein hydrogen bonds) whereas values more positive than -4.5 ppb/K are usually observed for amides participating in intramolecular hydrogen bonds (Cierpicki *et al*, 2002). Here, we used NMR to measure $^1\text{H}^{\text{N}}$ resonances over a range of temperatures (288K, 293K, 298K, 303K, 308K). The temperature coefficient was calculated by linear regression analysis. The temperature

coefficient values at each non-proline backbone resolved position suggest that the presence of 1,6-hexanediol induces a modest shift towards less negative values suggesting that some amino acids form a slightly different network of hydrogen bonds (**Figure 5A**). This difference in temperature coefficients is illustrated in (**Figure 5B**) where different amino acid types are color coded. We observed that certain amino acid types like serines and tyrosines known for their hydrogen-bonding capacity (Murthy *et al*, 2019) are showing the largest difference between the two solvent environments. Glutamines are also showing modest increase in temperature coefficient although the effect is less obvious compared to tyrosines and serines. It is important to note that the chemical shifts of FUS change linearly as a function of temperature which allows for a linear fit of good quality to be applied as the R-squared values indicate (**Figure 5C**). In general, in the presence of hexanediol there is a general tendency for the temperature coefficient to shift towards more positive values with only few exceptions. This pattern of ^1H temperature coefficient could indicate that hexanediol enhances solvation by introducing more contacts between the solvent and the protein as observed by quantification of protein-water hydrogen-bonding. Taken together, these data suggest that condensate-modifying molecules like hexanediol might enhance the solvation of the protein backbone leading to dissolution of the condensates.

Discussion

Deciphering how the internal structure and dynamics of various types of condensates depend on the physicochemical properties of their solvent is essential to engineering novel compounds that could potentially reverse the aberrant effects of pathological condensation.

In this study, we demonstrated that aliphatic alcohols of different lengths and configurations cause weak and evenly distributed chemical shift perturbations on FUS SYGQ LC. Moreover, our findings show a correlation between the atomic-level impact of alkanediol treatment on the chemical environment experienced by a disordered protein and the impact on phase separation. Indeed, 2,5-hexanediol is less effective than 1,6 hexanediol in dissolving

nuclear speckles and subsequent recruitment of a proline-glutamine rich splicing factor (Levone et al, 2021) and melting FUS LC hydrogels and intracellular puncta (Kato & McKnight, 2018), and it shows the least impact on FUS chemical environment (**Figure 1**). However, unlike earlier biophysical studies on FG-rich nucleoporins and the synaptonemal complex (SC) that suggested that the capacity of aliphatic alcohols to dissolve the NPC and SC is highly correlated with the hydrophobicity of each diol (Ribbeck et al, 2002; Rog et al, 2017), we found that a diol more hydrophilic than 1,6-hexanediol (1,4-butanediol) and a diol slightly more hydrophobic (2,5-hexanediol) were the least effective in disrupting FUS SYGQ LC LLPS. Furthermore, the long spacing between the hydroxyl groups in the 1,6 hexanediol isomer is not critical for disrupting LLPS, as 1,2 hexanediol has similar impact on phase separation and FUS chemical environment by NMR. Given that aliphatic alcohols reduce the surface tension of their chemical environments (Romero et al, 2007) we calculated temperature coefficients that can report on whether 1,6-hexanediol alters the overall solvation of FUS SYGQ and we found that all residue backbone positions especially those of serines and tyrosines are more likely to be better solvated in a solution high in 1,6-hexanediol, linking the effect of these compounds on water properties like surface tension to their effect on protein water solvation. Our observations of increased of protein-water interactions and increased molecular motions probed by R_2 measurements at 5% 1,6 hexanediol is distinct from previous observations of the ordering of a particular unstructured region in a protein crystal caused by very high (60%) hexanediol concentrations (Buhrman et al, 2003), though the changes due to the cosolvent both here and in that study are thought to arise from changes in water structure and not specific hexanediol-protein interactions. Given the established role of tyrosine contacts in phase separation as well as in the pre-phase separated peptide (Martin *et al*, 2020), it is surprising that larger shifts are not observed for tyrosine sidechain positions. However, it is interesting to note however that the largest ^{13}C shifts perturbations are observed for ^{13}CO positions including glutamine sidechains,

which we previously showed contribute markedly to FUS phase separation via hydrogen bonds and other interaction modes (Murthy *et al*, 2019).

Considering that RNA is a major contributor in phase-separation of RNA-binding proteins (Van Treeck *et al*, 2018, Forman-Kay *et al*, 2022), we examined whether complex coacervation mediated by FUS-RNA contacts can be blocked by hexanediol. Our data show that the alkanediol-sensitivity of FUS condensates enriched in RNA is clearly reduced (**Figure 2**), underscoring that such electrostatic interactions mediated by arginine-specific contacts are not impacted by amphiphilic alcohols. A series of studies on chromatin behavior in cells under the effect of 1,6-hexanediol or 2,5-hexanediol showed that these alcohols actually enhance interactions, condensing and suppressing the mobility of chromatin (Itoh *et al*, 2021). Furthermore, 1,6-hexanediol was suggested to enhance cation- π effects between negatively charged chromatin and cations of magnesium (Itoh *et al*, 2021). These observations are reminiscent of the enhanced phase separation of RGG3-RNA condensates in the presence of 1,2-hexanediol in our study, yet occur in the absence of magnesium. Thus, the contribution of hexanediol is context dependent and results of simplified *in vitro* experiments should be interpreted with a careful consideration of the condensate composition (e.g sequence characteristics and nucleic acid partitioning). Furthermore, we shown an inability of 5% 1,6-hexanediol to disrupt RGG-RNA condensates and much smaller effects on FUS-full length phase separation with RNA. Therefore, although hexanediol-dependent dissolution can reliably be used to distinguish solid from liquid forms of particular membraneless organelles (Kroschwald *et al*, 2017), it may be possible that certain membraneless organelles (e.g. stabilized primarily by RGG-RNA contacts) may indeed be liquid though not susceptible to 1,6-hexanediol. Conversely, the number of membraneless organelles found to be susceptible to 1,6-hexanediol may also therefore imply that these are not primarily stabilized by RGG-RNA contacts. Finally, it will be interesting to directly probe why 1,6-hexanediol can disrupt phase

separation of a histidine-rich disordered domain but not its interactions with RNA-polymerase II C-terminal domain (Lu et al, 2018).

Given the expanding roles of biocondensates in many physiological processes(Lyon *et al*, 2021) and in disease(Alberti & Hyman, 2021; Jiang *et al*, 2020; Alberti & Dormann, 2019; Lu *et al*, 2021), many efforts have focused on understanding how to modulate phase separation and how potential small molecule therapeutics partition into condensates(Dai *et al*, 2021; Wheeler *et al*, 2019; Klein *et al*, 2020). For example, mitoxantrone and other chemotherapy drugs with targets that reside in nuclear condensates were found to be selectively concentrated in condensates formed by nuclear proteins(Klein *et al*, 2020). This selective concentration may be due direct interactions between the compound and the disordered protein – although these direct interactions are weak they show similarly sized NMR chemical shift perturbations (Wheeler *et al*, 2019) at 3 orders of magnitude lower concentrations (500 μ M vs ~400 mM) than perturbations generated by alkanediols (**Figure 3 and 4**). Therefore, our efforts support the view that alkanediols impact protein solvation (**Figure 5**) and hence are not likely provide a useful chemical scaffold that can be elaborated to specifically and more potently dissolve puncta for therapeutic development. Still, our results show that NMR-based observations can provide unique insight into the molecular origins of phase separation modulation and could contribute to the rational design of possible therapies for altering disordered protein phase separation.

Acknowledgements

We thank Dr. Mandar Naik for NMR assistance and the Structural Biology Core Facility at Brown University. Research was supported in part by Human Frontier Science Program RGP0045/2018 (to N.L.F) and NSF MCB 1845734 (to N.L.F.). A.C.M. was supported in part by NIGMS training grant to the MCB graduate program at Brown University (T32GM136566) and NSF graduate fellowship (1644760, to A.C.M.). This content solely reflects the authors and does not necessarily represent the official views of the funding agencies.

Author contributions

T.M.P., A.C.M., and N.L.F. designed, performed, and analyzed data for NMR spectroscopy, microscopy, phase separation assays. T.M.P. and N.L.F wrote the manuscript with contributions from all authors.

Conflict of Interest Statement

N.L.F is a member of the scientific advisory board of Dewpoint Therapeutics. A.C.M is currently employed by Genentech Inc. The authors declare no other conflicts of interest.

Experimental procedures

General Information

1,2-hexanediol (CAT #213691), 1,6-cyclohexanediol (CAT #141712), 1,6-hexanediol (CAT #240117), 2,5-hexanediol (CAT #H11904), 1,4-butanediol (CAT #493732) and 1,5-pentanediol (CAT #P7703) were purchased from Sigma Aldrich. Hexanediol compounds were dissolved in 50 mM MES 150 mM NaCl pH 5.5 at 5% (w/v) for all experiments unless otherwise noted.

Protein Purification

FUS SYQG LC containing a TEV cleavable N-terminal histidine tag (RP1B FUS LC, AddGene #127192), full-length FUS with an N-terminal histidine tag and maltose-binding protein fusion (pTHMT FUS 1-526, AddGene #98651), and FUS RGG3 with N-terminal histidine tag and MBP fusion (pTHMT FUS RGG3 (453-507)) were expressed in *Escherichia coli* and grown at 37°C to an OD of 0.60-0.90 before induction with 1 mM IPTG for 4 hours. Isotopically labeled protein was produced by expression in M9 minimal media supplemented with ¹⁵N-ammonium chloride or ¹³C-glucose (Cambridge Isotopes). His-FUS LC was purified as previously described (Monahan et al, 2017, Murthy et al, 2019). In brief, cells were lysed using an Avestin homogenizer and the lysate was cleared by centrifugation at 20,000 rpm for 1 hour. The insoluble fraction was applied to a 5 mL HisTrap column (Cytiva) equilibrated with 8M urea 20 mM NaPi pH 7.4 300 mM NaCl 10 mM imidazole and eluted with a gradient from 10-300 mM imidazole. The protein was diluted with 20 mM NaPi pH 7.4 such that the final urea concentration was 1M and incubated with TEV protease over-night. A subtractive nickel affinity

step was performed, and the protein was buffer exchanged into 20 mM CAPS pH 11.0 and concentrated for storage. MBP-FUS 1-526 was purified as previously described (Burke *et al*, 2015). MBP-FUS RGG3 was purified as previously described (Murthy *et al*, 2021).

Phase separation assays

Phase separation of FUS LC in the presence of hexanediols was quantified by measuring the absorbance at 280 nm of the dilute phase using a NanoDrop spectrophotometer. Samples were prepared by diluting FUS LC stored in 20 mM CAPS pH 11.0 to a final protein concentration of 200 μ M into 20 mM MES (pH adjusted with Bis-Tris) pH 5.5 150 mM NaCl with and without hexanediols. After dilution, samples were spun at 14,000g for 10 minutes at 22°C.

Turbidity of MBP-FL and RGG3 was measured as previously described (Murthy *et al*, 2021) by measuring the absorbance at 600 nm over time of samples in a 96-well clear plate (Costar) using a Cytation 5 Cell Imaging Multi-Mode Reader (BioTek). To remove background absorbance, the turbidity of a no TEV control (replaced with TEV storage buffer) for each condition was subtracted from the turbidity of the experimental conditions. Experiments were conducted in triplicate and averaged. To test the effect of different alkanediols on RNA-FUS phase separation, the polyadenylic acid (polyA) was desalted into the appropriate buffer using a Zeba 0.5 ml spin column.

Microscopy

Visualization of phase separation of FUS LC, MBP-FUS FL and FUS RGG3 was performed by differential interference contrast microscopy on a Zeiss Axiovert 200M Fluorescence microscope. All samples were spotted on a coverslip for imaging. Images were processed using ImageJ (NIH).

NMR spectroscopy

NMR experiments were recorded at 850 MHz using a Bruker Avance III spectrometer with a $^1\text{H}/^{15}\text{N}/^{13}\text{C}$ TCI cryoprobe and z field gradient coil. NMR titrations of ^{15}N -labeled FUS LC with 0, 2.5 or 5% hexanediols were conducted at 25°C in 50 mM MES, 150 mM NaCl pH 5.5

including 10% $^2\text{H}_2\text{O}$. All data were processed with NMRPipe software package (Delaglio *et al*, 1995) and visualized with NMRFAM-Sparky (Lee *et al*, 2015). Chemical shifts and intensity ratios were normalized by subtracting the ^{15}N chemical shift values and dividing the signal intensity of the no hexanediol condition from all other datasets. Molecular motions in the presence of 1,6-hexanediol were probed using ^{15}N R_1 , ^{15}N R_2 and heteronuclear NOE experiments using standard pulse sequences (hsqct2etf3gpsitc3d, hsqct1etf3gpsitc3d, hsqcnoef3gps, respectively from Bruker Topspin 3.2). Interleaved experiments comprised 256 x 4096 total points in the indirect ^{15}N and direct ^1H dimensions, respectively, with corresponding acquisition times of 74 ms and 229 ms, sweep width of 20 ppm and 10.5 ppm, centered at 117 ppm and 4.7 ppm, respectively. ^{15}N R_2 experiments had an interscan delay of 2.5 s, a Carr-Purcell-Mei-boom-Gill (CPMG) field of 556 Hz, and total R_2 relaxation CPMG loop-lengths of 16.5 ms, 264.4 ms, 181.8 ms, 33.1 ms, 115.7 ms, 82.6 ms, and 165.3 ms. ^{15}N R_1 experiments had an interscan delay of 1.2 s, and total R_1 relaxation loop-lengths of 100 ms, 1000 ms, 200 ms, 800 ms, 300 ms, 600 ms, and 400 ms. Heteronuclear NOE experiments were conducted with an interscan delay of 5 s.

Temperature coefficient calculations

NMR titrations of ^{15}N -labeled FUS LC with 0, 2.5 or 5% hexanediols were conducted at 288K, 293K, 298K, 303K and 308K. Linear fits of chemical shifts as a function of temperature were obtained and the temperature coefficient was extracted as the gradient (slope of linear fits) by using a linear least-squares regression algorithm and assuming residual normality.

References

- Alberti, S., & Dormann, D. (2019). Liquid-Liquid Phase Separation in Disease. *Annu. Rev. Genet.*, 53, 171–194.
- Alberti, S., & Hyman, A. A. (2021). Biomolecular condensates at the nexus of cellular stress, protein aggregation disease and ageing. *Nat. Rev. Mol. Cell Biol.*, 22(3), 196–213.
- Altmeyer, M., Neelsen, K. J., Teloni, F., Pozdnyakova, I., Pellegrino, S., Grøfte, M., Rask, M. D., Streicher, W., Jungmichel, S., Nielsen, M. L., & Lukas, J. (2015). Liquid demixing of intrinsically disordered proteins is seeded by poly(ADP-ribose). *Nat. Commun.*, 6, 8088.

- Babinchak, W. M., Dumm, B. K., Venus, S., Boyko, S., Putnam, A. A., Jankowsky, E., & Surewicz, W. K. (2020). Small molecules as potent biphasic modulators of protein liquid-liquid phase separation. *Nat. Commun.*, *11*(1), 5574.
- Banani, S. F., Lee, H. O., Hyman, A. A., & Rosen, M. K. (2017). Biomolecular condensates: organizers of cellular biochemistry. *Nat. Rev. Mol. Cell Biol.*, *18*(5), 285–298.
- Baxter, N. J., & Williamson, M. P. (1997). Temperature dependence of ¹H chemical shifts in proteins. *J. Biol. NMR.*, *9*(4), 359–369.
- Berkeley, R. F., Kashefi, M., & Debelouchina, G. T. (2021). Real-time observation of structure and dynamics during the liquid-to-solid transition of FUS LC. *Biophys. J.*, *120*(7), 1276–1287.
- Boija, A., Klein, I. A., & Young, R. A. (2021). Biomolecular Condensates and Cancer. *Cancer Cell*, *39*(2), 174–192.
- Buhrman, G., de Serrano, V., & Mattos, C. (2003). Organic solvents order the dynamic switch II in Ras crystals. *Structure*, *11*(7), 747–751.
- Burke, K. A., Janke, A. M., Rhine, C. L., & Fawzi, N. L. (2015). Residue-by-Residue View of In Vitro FUS Granules that Bind the C-Terminal Domain of RNA Polymerase II. *Mol. Cell.*, *60*(2), 231–241.
- Cheng, T., Zhao, Y., Li, X., Lin, F., Xu, Y., Zhang, X., Li, Y., Wang, R., & Lai, L. (2007). Computation of octanol-water partition coefficients by guiding an additive model with knowledge. *J. Chem. Inf. Model.*, *47*(6), 2140–2148.
- Chong, P. A., Vernon, R. M., & Forman-Kay, J. D. (2018). RGG/RG Motif Regions in RNA Binding and Phase Separation. *J. Mol. Biol.*, *430*(23), 4650–4665.
- Cierpicki, T., & Otlewski, J. (2001). Amide proton temperature coefficients as hydrogen bond indicators in proteins. *J. Biol. NMR.*, *21*(3), 249–261.
- Cierpicki, T., Zhukov, I., Byrd, R. A., & Otlewski, J. (2002). Hydrogen bonds in human ubiquitin reflected in temperature coefficients of amide protons. *J. Magn. Reson.*, *157*(2), 178–180.
- Dai, B., Zhong, T., Chen, Z. X., Chen, W., Zhang, N., Liu, X. L., Wang, L. Q., Chen, J., & Liang, Y. (2021). Myricetin slows liquid-liquid phase separation of Tau and activates ATG5-dependent autophagy to suppress Tau toxicity. *J. Biol. Chem.*, *297*(4), 101222.
- Daigle, J. G., Lanson, N. A., Jr, Smith, R. B., Casci, I., Maltare, A., Monaghan, J., Nichols, C. D., Kryndushkin, D., Shewmaker, F., & Pandey, U. B. (2013). RNA-binding ability of FUS regulates neurodegeneration, cytoplasmic mislocalization and incorporation into stress granules associated with FUS carrying ALS-linked mutations. *H. Mol. Gen.*, *22*(6), 1193–1205.
- Delaglio, F., Grzesiek, S., Vuister, G. W., Zhu, G., Pfeifer, J., & Bax, A. (1995). NMRPipe: a multidimensional spectral processing system based on UNIX pipes. *J. Biol. NMR.*, *6*(3), 277–293.

- Deng, H., Gao, K., & Jankovic, J. (2014). The role of FUS gene variants in neurodegenerative diseases. *Nat. Rev. Neurol.* 10(6), 337–348.
- Düster, R., Kalthener, I. H., Schmitz, M., & Geyer, M. (2021). 1,6-Hexanediol, commonly used to dissolve liquid-liquid phase separated condensates, directly impairs kinase and phosphatase activities. *J. Biol. Chem.*, 296, 100260.
- Fuller, G. G., Han, T., Freeberg, M. A., Moresco, J. J., Ghanbari Niaki, A., Roach, N. P., Yates, J. R., 3rd, Myong, S., & Kim, J. K. (2020). RNA promotes phase separation of glycolysis enzymes into yeast G bodies in hypoxia. *eLife*, 9, e48480.
- Forman-Kay, J. D., Ditlev, J. A., Nosella, M. L., & Lee, H. O. (2022). What are the distinguishing features and size requirements of biomolecular condensates and their implications for RNA-containing condensates?. *RNA*, 28(1), 36-47.
- Hofweber, M., Hutten, S., Bourgeois, B., Spreitzer, E., Niedner-Boblenz, A., Schifferer, M., Ruepp, M. D., Simons, M., Niessing, D., Madl, T., & Dormann, D. (2018). Phase Separation of FUS Is Suppressed by Its Nuclear Import Receptor and Arginine Methylation. *Cell*, 173(3), 706–719.e13.
- Itoh, Y., Iida, S., Tamura, S., Nagashima, R., Shiraki, K., Goto, T., Hibino, K., Ide, S., & Maeshima, K. (2021). 1,6-hexanediol rapidly immobilizes and condenses chromatin in living human cells. *Life Sc. Alliance*, 4(4), e202001005.
- Jäggi, R. D., Franco-Obregón, A., Mühlhäusser, P., Thomas, F., Kutay, U., & Ensslin, K. (2003). Modulation of nuclear pore topology by transport modifiers. *Biophys. J.*, 84(1), 665–670.
- Jiang, S., Fagman, J. B., Chen, C., Alberti, S., & Liu, B. (2020). Protein phase separation and its role in tumorigenesis. *eLife*, 9, e60264.
- Kato, M., & McKnight, S. L. (2018). A Solid-State Conceptualization of Information Transfer from Gene to Message to Protein. *Annu. Rev. Biochem.*, 87, 351–390.
- Kay, L. E., Ikura, M., Tschudin, R., & Bax, A. (1990). Three-dimensional triple-resonance NMR Spectroscopy of isotopically enriched proteins. *J. Magn. Reson.*, 213(2).
- Klein, I. A., Boija, A., Afeyan, L. K., Hawken, S. W., Fan, M., Dall'Agnesse, A., Oksuz, O., Henninger, J. E., Shrinivas, K., Sabari, B. R., Sagi, I., Clark, V. E., Platt, J. M., Kar, M., McCall, P. M., Zamudio, A. V., Manteiga, J. C., Coffey, E. L., Li, C. H., Hannett, N. M., ... Young, R. A. (2020). Partitioning of cancer therapeutics in nuclear condensates. *Science*, 368(6497), 1386–1392.
- Krainer, G., Welsh, T. J., Joseph, J. A., Espinosa, J. R., Wittmann, S., de Csilléry, E., Sridhar, A., Toprakcioglu, Z., Gudiškytė, G., Czekalska, M. A., Arter, W. E., Guillén-Boixet, J., Franzmann, T. M., Qamar, S., George-Hyslop, P. S., Hyman, A. A., Collepardo-Guevara, R., Alberti, S., & Knowles, T. (2021). Reentrant liquid condensate phase of proteins is stabilized by hydrophobic and non-ionic interactions. *Nat. Commun.*, 12(1), 1085.
- Kroschwald, S., Maharana, S., Mateju, D., Malinowska, L., Nüske, E., Poser, I., Richter, D., & Alberti, S. (2015). Promiscuous interactions and protein disaggregases determine the material state of stress-inducible RNP granules. *eLife*, 4, e06807.

Kroschwald, S., Maharana, S., & Simon, A. (2017). Hexanediol: a chemical probe to investigate the material properties of membrane-less compartments. *Matters*, 3(5), e201702000010.

Lee, W., Tonelli, M., & Markley, J. L. (2015). NMRFAM-SPARKY: enhanced software for biomolecular NMR spectroscopy. *Bioinformatics*, 31(8), 1325–1327.

Levone, B. R., Lenzken, S. C., Antonaci, M., Maiser, A., Rapp, A., Conte, F., ... & Barabino, S. M. (2021). FUS-dependent liquid–liquid phase separation is important for DNA repair initiation. *J. Cell Biol.*, 220(5).

Li, S., Yoshizawa, T., Yamazaki, R., Fujiwara, A., Kameda, T., & Kitahara, R. (2021). Pressure and Temperature Phase Diagram for Liquid-Liquid Phase Separation of the RNA-Binding Protein Fused in Sarcoma. *J. Phys. Chem*, 125(25), 6821–6829.

Lin, Y., Mori, E., Kato, M., Xiang, S., Wu, L., Kwon, I., & McKnight, S. L. (2016). Toxic PR Poly-Dipeptides Encoded by the C9orf72 Repeat Expansion Target LC Domain Polymers. *Cell*, 167(3), 789–802.e12.

Liu, X., Jiang, S., Ma, L., Qu, J., Zhao, L., Zhu, X., & Ding, J. (2021). Time-dependent effect of 1,6-hexanediol on biomolecular condensates and 3D chromatin organization. *Genome Biol.*, 22(1), 230.

Loughlin, F. E., Lukavsky, P. J., Kazeeva, T., Reber, S., Hock, E. M., Colombo, M., Von Schroetter, C., Pauli, P., Cléry, A., Mühlemann, O., Polymenidou, M., Ruepp, M. D., & Allain, F. H. (2019). The Solution Structure of FUS Bound to RNA Reveals a Bipartite Mode of RNA Recognition with Both Sequence and Shape Specificity. *Mol. Cell*, 73(3), 490–504.e6.

Lu, J., Qian, J., Xu, Z., Yin, S., Zhou, L., Zheng, S., & Zhang, W. (2021). Emerging Roles of Liquid-Liquid Phase Separation in Cancer: From Protein Aggregation to Immune-Associated Signaling. *Front. Cell Dev. Biol.*, 9, 631486.

Lu, H., Yu, D., Hansen, A. S., Ganguly, S., Liu, R., Heckert, A., ... & Zhou, Q. (2018). Phase-separation mechanism for C-terminal hyperphosphorylation of RNA polymerase II. *Nature*, 558(7709), 318–323.

Lyon, A. S., Peeples, W. B., & Rosen, M. K. (2021). A framework for understanding the functions of biomolecular condensates across scales. *Nat. Rev. Mol. Cell Biol.*, 22(3), 215–235.

Martin, E. W., Holehouse, A. S., Peran, I., Farag, M., Incicco, J. J., Bremer, A., Grace, C. R., Soranno, A., Pappu, R. V., & Mittag, T. (2020). Valence and patterning of aromatic residues determine the phase behavior of prion-like domains. *Science*, 367(6478), 694–699.

Ming, Y., Chen, X., Xu, Y., Wu, Y., Wang, C., Zhang, T., Mao, R., & Fan, Y. (2019). Targeting liquid-liquid phase separation in pancreatic cancer. *Translational Cancer research*, 8(1), 96–103.

Monahan, Z., Ryan, V. H., Janke, A. M., Burke, K. A., Rhoads, S. N., Zerze, G. H., O'Meally, R., Dignon, G. L., Conicella, A. E., Zheng, W., Best, R. B., Cole, R. N., Mittal, J., Shewmaker, F., & Fawzi, N. L. (2017). Phosphorylation of the FUS low-complexity domain disrupts phase separation, aggregation, and toxicity. *EMBO J.*, 36(20), 2951–2967.

Murthy, A. C., Tang, W. S., Jovic, N., Janke, A. M., Seo, D. H., Perdikari, T. M., Mittal, J., & Fawzi, N. L. (2021). Molecular interactions contributing to FUS SYGQ LC-RGG phase separation and co-partitioning with RNA polymerase II heptads. *Nat. Struct. Mol. Biol.*, 28(11), 923–935.

Murthy, A. C., Dignon, G. L., Kan, Y., Zerze, G. H., Parekh, S. H., Mittal, J., & Fawzi, N. L. (2019). Molecular interactions underlying liquid-liquid phase separation of the FUS low-complexity domain. *Nat. Struct. Mol. Biol.*, 26(7), 637–648.

Nair, S. J., Yang, L., Meluzzi, D., Oh, S., Yang, F., Friedman, M. J., Wang, S., Suter, T., Alshareedah, I., Gamliel, A., Ma, Q., Zhang, J., Hu, Y., Tan, Y., Ohgi, K. A., Jayani, R. S., Banerjee, P. R., Aggarwal, A. K., & Rosenfeld, M. G. (2019). Phase separation of ligand-activated enhancers licenses cooperative chromosomal enhancer assembly. *Nat. Struct. Mol. Biol.*, 26(3), 193–203.

Owen, I., Yee, D., Wyne, H., Perdikari, T. M., Johnson, V., Smyth, J., Kortum, R., Fawzi, N. L., & Shewmaker, F. (2021). The oncogenic transcription factor FUS-CHOP can undergo nuclear liquid-liquid phase separation. *J. Cell Sci.*, 134(17), jcs258578.

Palmer, A. G., 3rd, Kroenke, C. D., & Loria, J. P. (2001). Nuclear magnetic resonance methods for quantifying microsecond-to-millisecond motions in biological macromolecules. *Meth. Enzymol.*, 339, 204–238.

Patel, A., Lee, H. O., Jawerth, L., Maharana, S., Jahnel, M., Hein, M. Y., Stoykov, S., Mahamid, J., Saha, S., Franzmann, T. M., Pozniakovski, A., Poser, I., Maghelli, N., Royer, L. A., Weigert, M., Myers, E. W., Grill, S., Drechsel, D., Hyman, A. A., & Alberti, S. (2015). A Liquid-to-Solid Phase Transition of the ALS Protein FUS Accelerated by Disease Mutation. *Cell*, 162(5), 1066–1077.

Patel, S. S., Belmont, B. J., Sante, J. M., & Rexach, M. F. (2007). Natively unfolded nucleoporins gate protein diffusion across the nuclear pore complex. *Cell*, 129(1), 83–96.

Ribbeck, K., & Görlich, D. (2002). The permeability barrier of nuclear pore complexes appears to operate via hydrophobic exclusion. *EMBO J.*, 21(11), 2664–2671.

Roden, C., & Gladfelter, A. S. (2021). RNA contributions to the form and function of biomolecular condensates. *Nat. Rev. Mol. Cell Biol.*, 22(3), 183–195.

Rog, O., Köhler, S., & Dernburg, A. F. (2017). The synaptonemal complex has liquid crystalline properties and spatially regulates meiotic recombination factors. *Elife*, 6, e21455.

Romero, C. M., Páez, M. S., Miranda, J. A., Hernández, D. J., & Oviedo, L. E. (2007). Effect of temperature on the surface tension of diluted aqueous solutions of 1, 2-hexanediol, 1, 5-hexanediol, 1, 6-hexanediol and 2, 5-hexanediol. *Fluid Phase Equil.*, 258(1), 67–72.

Ryan, V. H., & Fawzi, N. L. (2019). Physiological, Pathological, and Targetable Membraneless Organelles in Neurons. *Trends Neurosci.*, 42(10), 693–708.

Schmidt, H. B., Jaafar, Z. A., Rodencal, J., Leonetti, M. D., Dixon, S. J., Rohatgi, R., & Brandman, O. (2021). Oxaliplatin kills cells via liquid-liquid demixing of nucleoli. *bioRxiv doi: https://doi.org/10.1101/2021.06.10.447918*

Shi, M., You, K., Chen, T., Hou, C., Liang, Z., Liu, M., Wang, J., Wei, T., Qin, J., Chen, Y., Zhang, M. Q., & Li, T. (2021). Quantifying the phase separation property of chromatin-associated proteins under physiological conditions using an anti-1,6-hexanediol index. *Genome Biol.*, 22(1), 229.

Shulga, N., & Goldfarb, D. S. (2003). Binding dynamics of structural nucleoporins govern nuclear pore complex permeability and may mediate channel gating. *Mol. Cell. Biol.*, 23(2), 534–542.

Snead, W. T., & Gladfelter, A. S. (2019). The Control Centers of Biomolecular Phase Separation: How Membrane Surfaces, PTMs, and Active Processes Regulate Condensation. *Mol. Cell*, 76(2), 295–305.

Sutton, E. C., & DeRose, V. J. (2021). Early nucleolar responses differentiate mechanisms of cell death induced by oxaliplatin and cisplatin. *J. Biol. Chem.*, 296, 100633.

Trainor, K., Palumbo, J. A., MacKenzie, D., & Meiering, E. M. (2020). Temperature dependence of NMR chemical shifts: Tracking and statistical analysis. *Protein Science*, 29(1), 306–314.

Tulpule, A., Guan, J., Neel, D. S., Allegakoen, H. R., Lin, Y. P., Brown, D., Chou, Y. T., Heslin, A., Chatterjee, N., Perati, S., Menon, S., Nguyen, T. A., Debnath, J., Ramirez, A. D., Shi, X., Yang, B., Feng, S., Makhija, S., Huang, B., & Bivona, T. G. (2021). Kinase-mediated RAS signaling via membraneless cytoplasmic protein granules. *Cell*, 184(10), 2649–2664.e18.

Van Treeck, B., & Parker, R. (2018). Emerging roles for intermolecular RNA-RNA interactions in RNP assemblies. *Cell*, 174(4), 791-802.

Ulianov, S. V., Velichko, A. K., Magnitov, M. D., Luzhin, A. V., Golov, A. K., Ovsyannikova, N., Kireev, I. I., Gavrikov, A. S., Mishin, A. S., Garaev, A. K., Tyakht, A. V., Gavrillov, A. A., Kantidze, O. L., & Razin, S. V. (2021). Suppression of liquid-liquid phase separation by 1,6-hexanediol partially compromises the 3D genome organization in living cells. *Nucleic Acids Res.*, 49(18), 10524–10541.

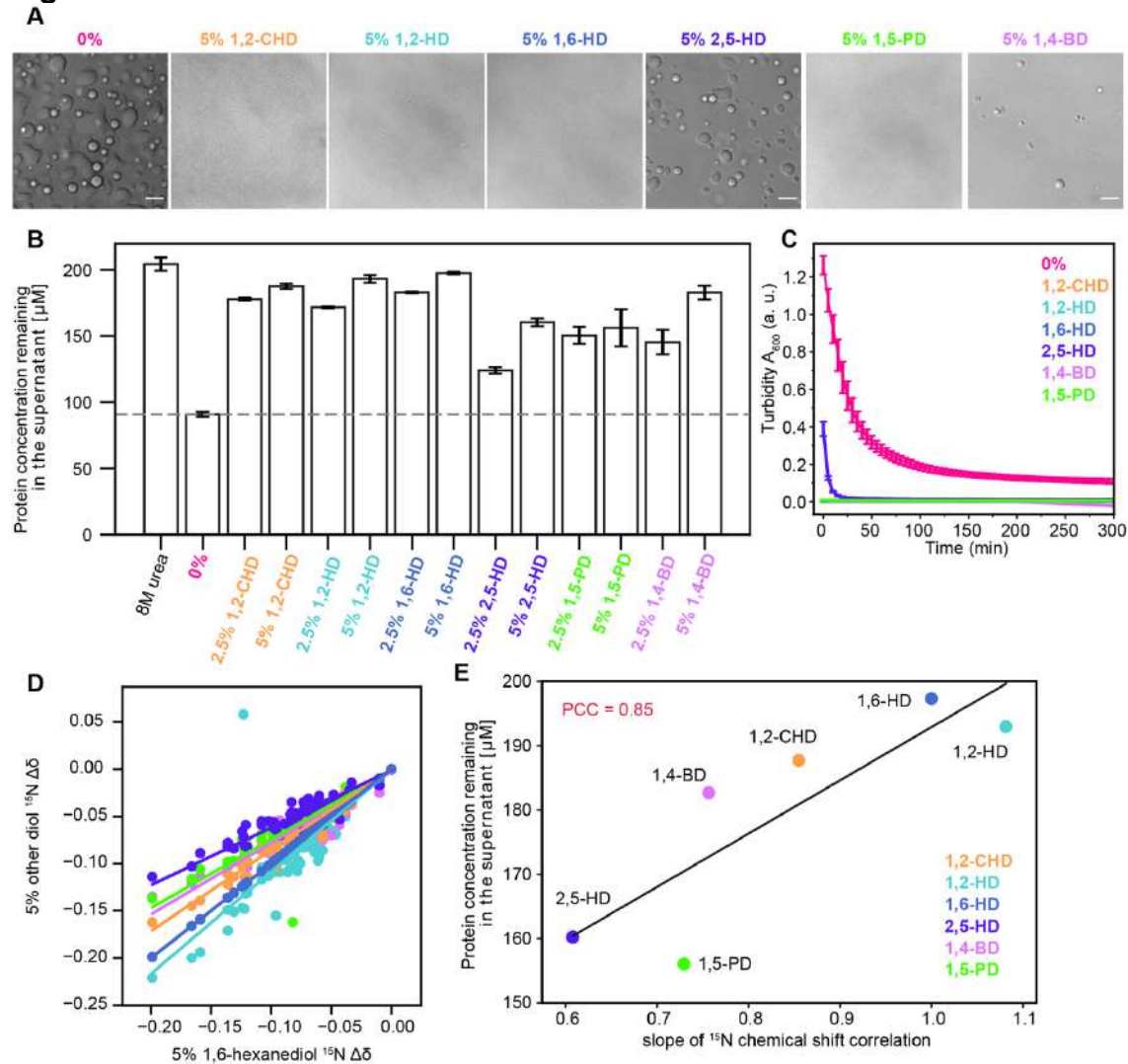
Wang, J., Choi, J. M., Holehouse, A. S., Lee, H. O., Zhang, X., Jahnel, M., Maharana, S., Lemaitre, R., Pozniakovskiy, A., Drechsel, D., Poser, I., Pappu, R. V., Alberti, S., & Hyman, A. A. (2018). A Molecular Grammar Governing the Driving Forces for Phase Separation of Prion-like RNA Binding Proteins. *Cell*, 174(3), 688–699.e16.

Wheeler, J. R., Matheny, T., Jain, S., Abrisch, R., & Parker, R. (2016). Distinct stages in stress granule assembly and disassembly. *eLife*, 5, e18413.

Wheeler, R. J., Lee, H. O., Poser, I., Pal, A., Doleman, T., Kishigami, S., ... & Hyman, A. A. (2019). Small molecules for modulating protein driven liquid-liquid phase separation in treating neurodegenerative disease. *bioRxiv doi:https://doi.org/10.1101/721001*

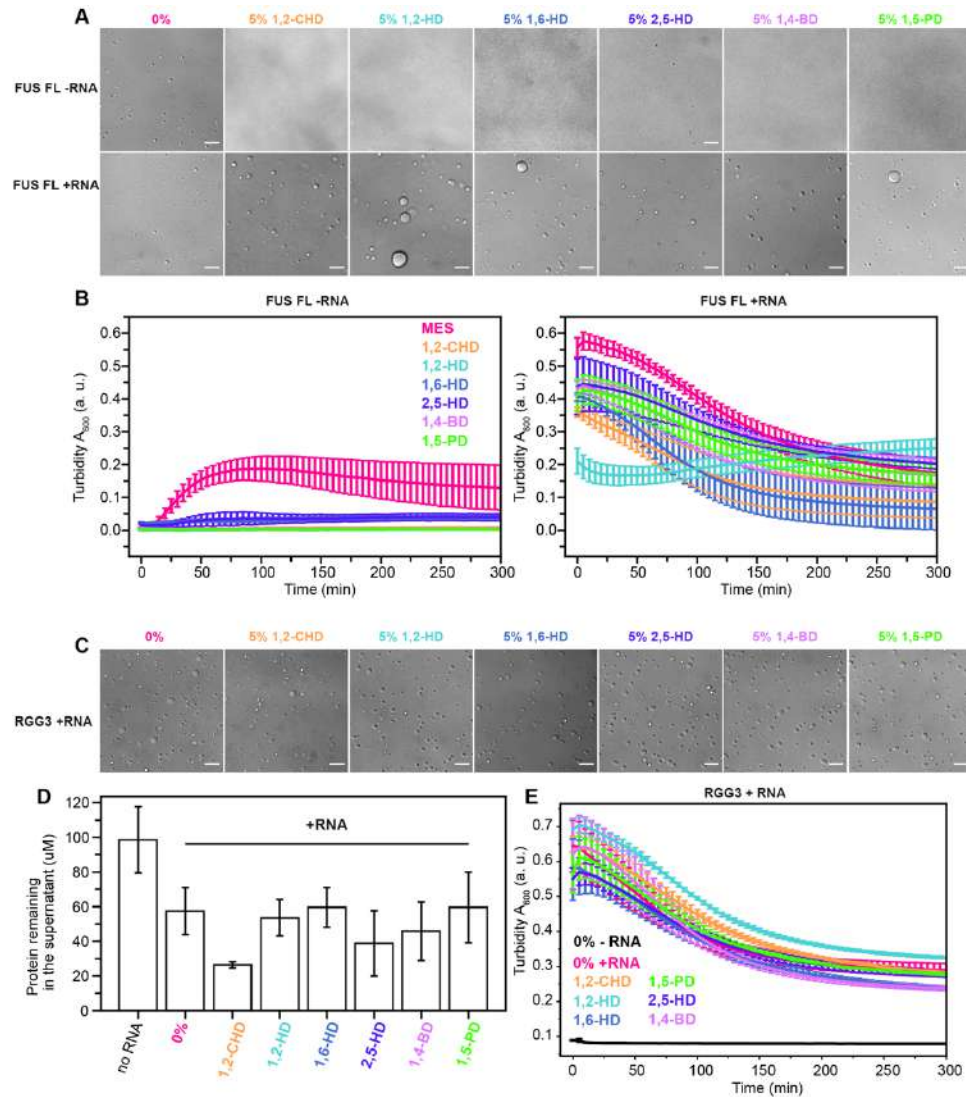
Wolozin, B., & Ivanov, P. (2019). Stress granules and neurodegeneration. *Nat. Rev. Neurosci.*, 20(11), 649–666.

Figure 1: Effect of alkanediols on FUS SYGQ LC LLPS and chemical environment



- DIC micrographs of 200 μM FUS SYGQ LC in buffer alone (50 mM MES pH 5.5, 150 mM NaCl) (control) or different alkanediols of various aliphatic chain length and conformation premixed with buffer at 5% w/v concentration. Scale bars represent 50 μm .
- Phase separation assay that measures the saturation concentration of FUS SYGQ LC in the presence of 2.5% or 5% of different alkanediols. Data are plotted as mean \pm s.d. of $n=3$ technical replicates.
- The effect of different alkanediols at 5% w/v, pH 5.5 on phase separation of 200 μM FUS SYGQ LC over time as tracked by light scattering at 600 nm. Error bars represent standard deviation of three replicates.
- Comparison of ^{15}N $\Delta\delta$ in 5% 1,6-hexanediol with every other co-solvent.
- Slope extracted from the correlation presented in (d) versus protein remaining in the supernatant shows that the chemical shift differences induced by each diol are correlated (PCC = 0.85) with the capacity of FUS SYGQ LC to phase separate in each condition. Solid black line represents a linear fit.

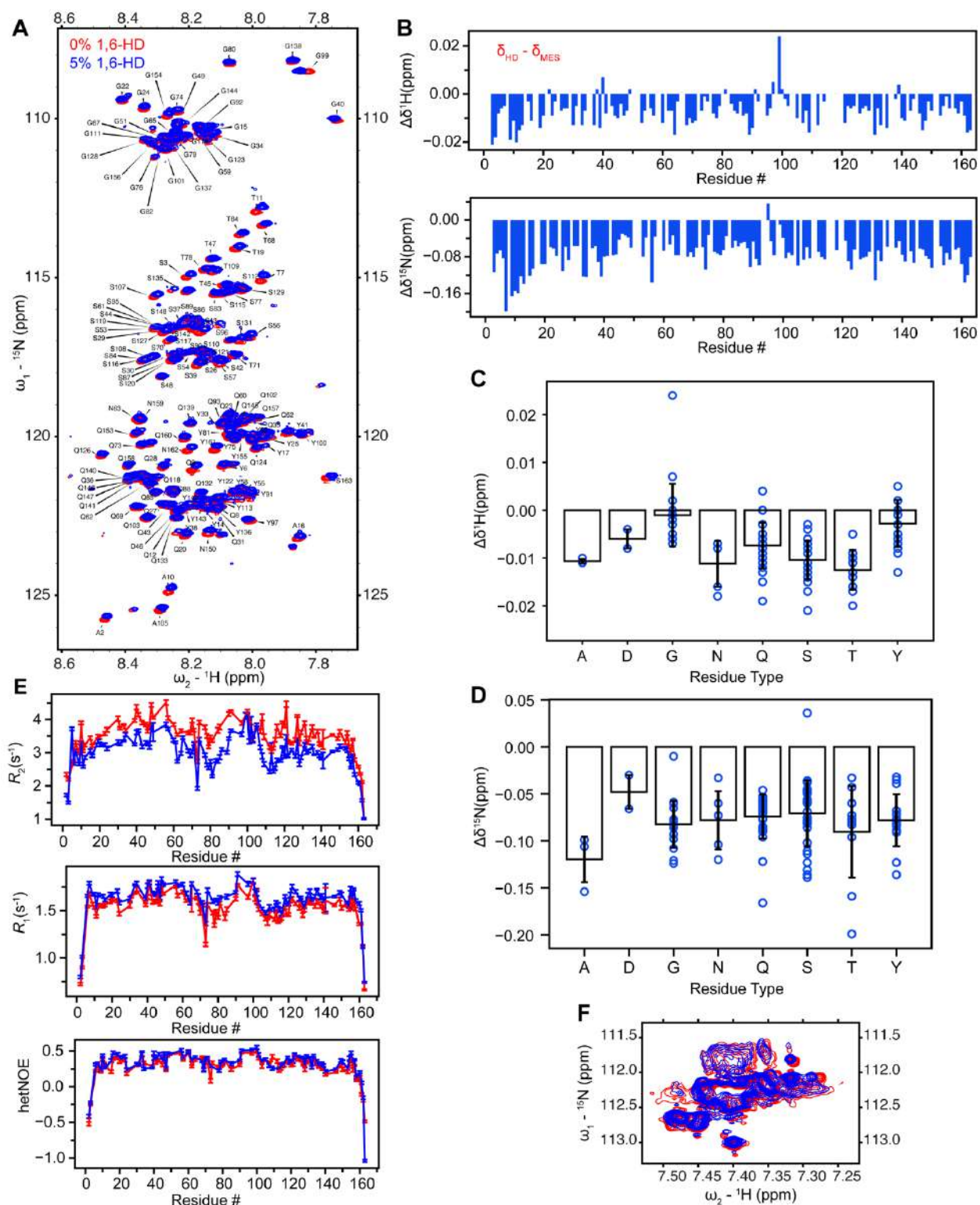
Figure 2: FUS RGG3-RNA rich droplets are insensitive to the treatment with alkanediols



- DIC micrographs of 5 μ M FUS full-length without (top) and with (bottom) polyadenylic acid (0.27 mg/ml polyA) after treatment with 5% w/v premixed solutions of aliphatic alcohols and addition of TEV protease. Scale bars represent 50 μ m.
- Phase separation of 5 μ M FUS full-length without (left) and with (right) polyA RNA over the course of 5 hours as measured by light scattering at 600 nm. Error bars represent standard deviation of three replicates.
- DIC micrographs of 100 μ M FUS RGG3 (453-507) after the addition of 0.142 mg/ml of polyA RNA in different LLPS-modifying buffers.
- Saturation concentration of 100 μ M FUS RGG3 in the presence of polyA RNA (0.142 mg/ml) diluted in 50 mM MES pH 5.5, 150 mM NaCl, 5% w/v co-solvent. Data are plotted as mean \pm s.d. of n=3 technical replicates.

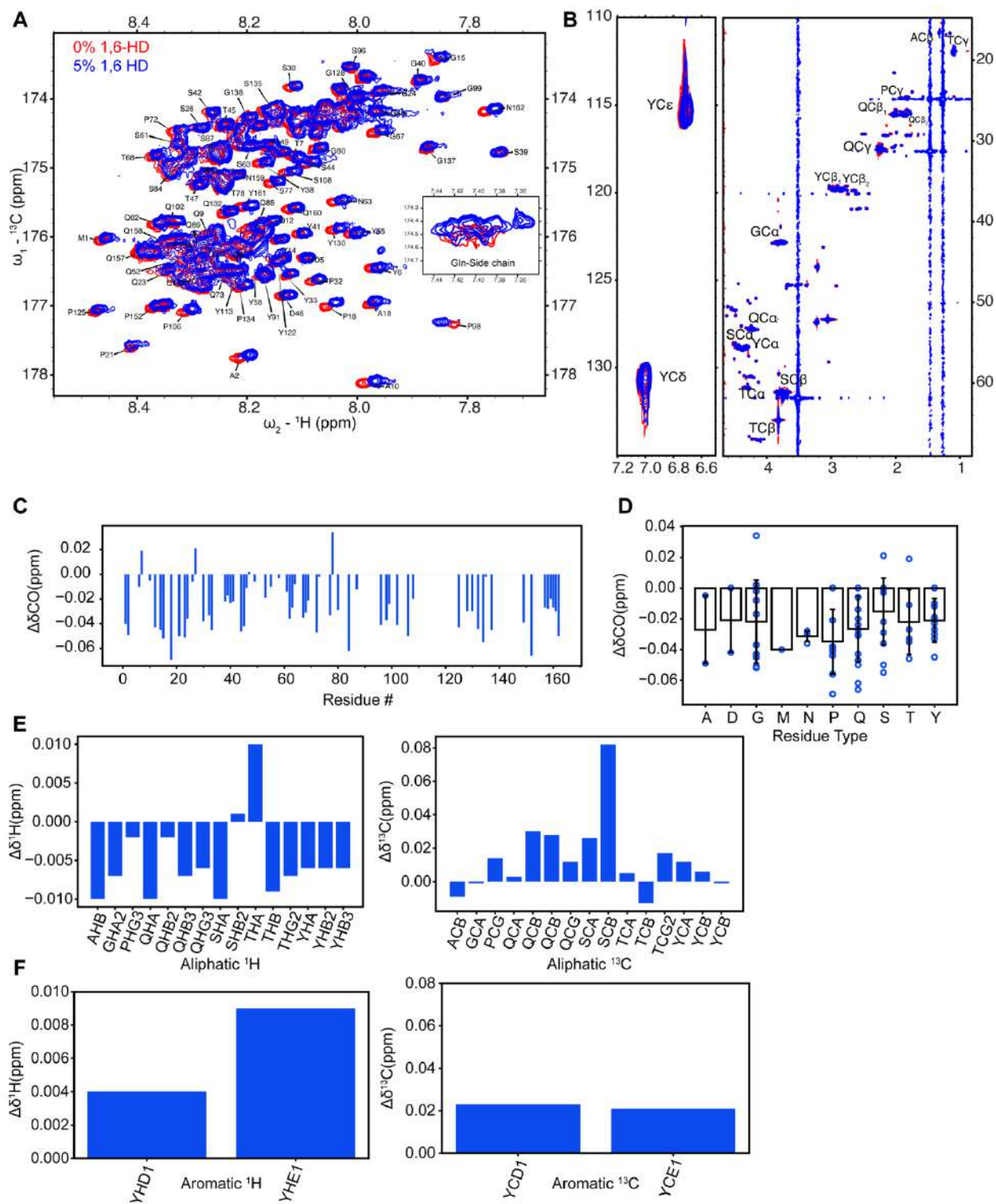
- e) The effect of different alkanediols at 5% w/v, pH 5.5 on phase separation of 100 μ M FUS RGG3 in the presence of RNA over time as tracked by light scattering at 600 nm. Error bars represent standard deviation of three replicates.

Figure 3: 1,6-hexanediol does not substantially alter the local disordered structure of FUS SYGQ LC but enhances reorientational molecular motion.



- a) ^1H - ^{15}N heteronuclear single quantum coherence (HSQC) spectrum of 30 μM FUS SYGQ LC in the absence (red) and in the presence (blue) of 5% 1,6-hexanediol. Solution conditions in all cases is 150 mM NaCl 50 mM MES pH 5.5.
- b) Addition of 5% 1,6 hexanediol induces only small ^1H and ^{15}N chemical shift deviations for FUS SYGQ LC.
- c-d) Chemical shift deviations of ^1H and ^{15}N of FUS SYGQ LC binned by residue type. Individual residues are plotted as blue marks. Bar plots represent mean and s.d. among all chemical shifts of each residue type.
- e) NMR spin relaxation parameters ^{15}N R_2 , ^{15}N R_1 and (^1H) ^{15}N heteronuclear NOE values for FUS SYGQ LC at 850 MHz ^1H frequency indicate slightly faster molecular motions in the presence of 1,6-hexanediol.
- f) ^{15}N side chain of glutamine and asparagine (^1H up field resonance region show as example) is modestly affected by 5% 1,6-hexanediol.

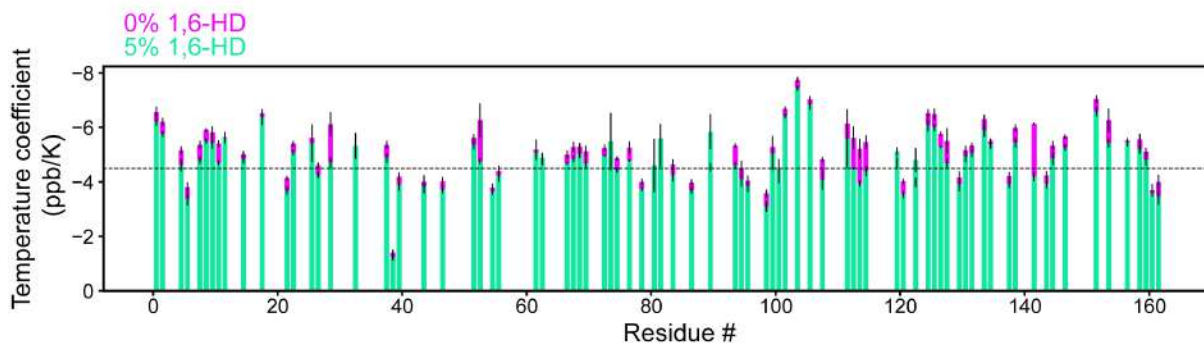
Figure 4: 1,6-hexanediol induces larger FUS SYGQ LC chemical shift perturbations at backbone carbonyl positions than aliphatic and aromatic sidechain positions.



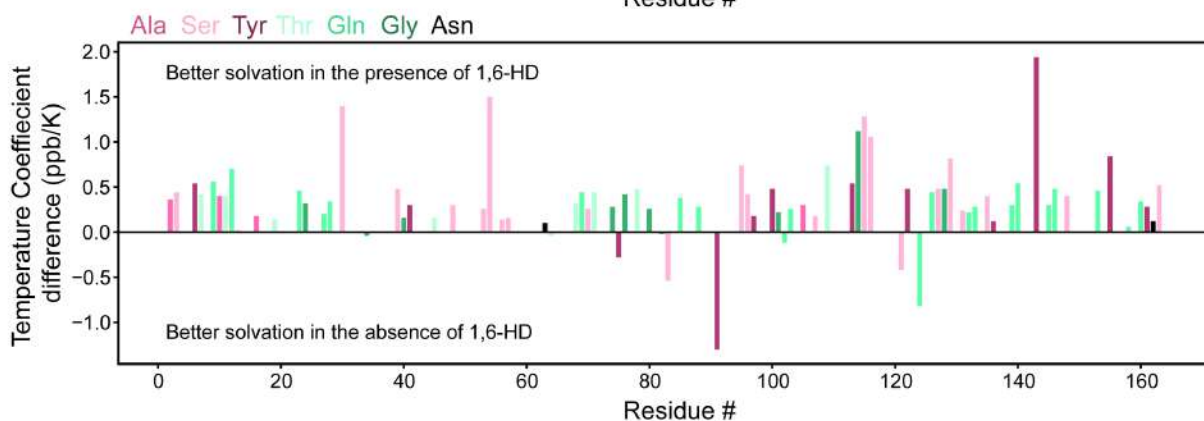
- a) ^1H - ^{13}C two-dimensional spectral overlay with (blue) and without (red) 5% w/v 1,6-hexanediol derived from a triple resonance HNCO experiment for 100 μM ^{15}N , ^{13}C labelled FUS SYGQ LC, 50 mM MES pH 5.5, 150mM NaCl. Inset corresponds to the ^{13}C side-chain of glutamine.
- b) ^{13}C HSQC of 100 μM ^{15}N , ^{13}C labelled FUS SYGQ LC, 50 mM MES pH 5.5, 150mM NaCl with (blue) and without (red) 1,6-hexanediol.
- c) Chemical shift deviations of ^{13}CO at each assigned backbone position.
- d) Chemical shift deviations of ^{13}CO binned by residue type.
- e) Chemical shift deviations of aliphatic ^1H (left) and ^{13}C (right) positions.
- f) Chemical shift deviations of aromatic tyrosine ^1H (left) and ^{13}C (right) positions.

Figure 5: 1,6-hexanediol modestly alters the solvation profile of FUS SYQC LC

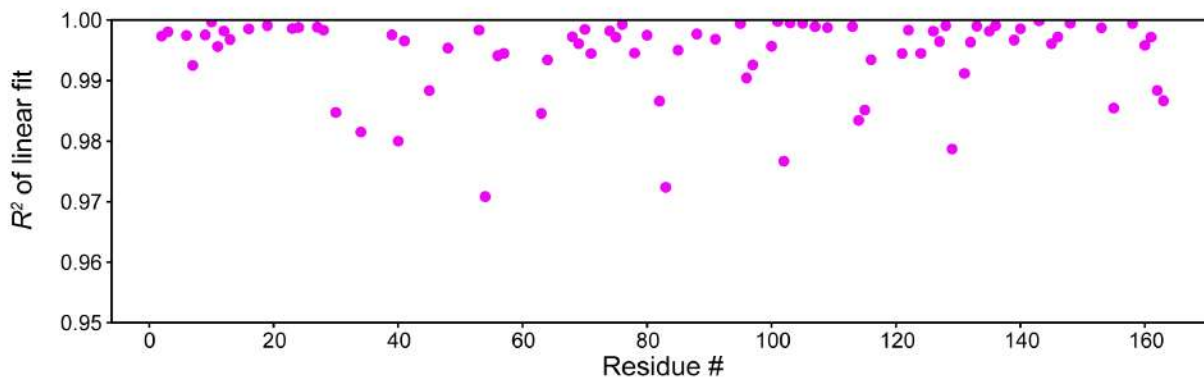
A



B



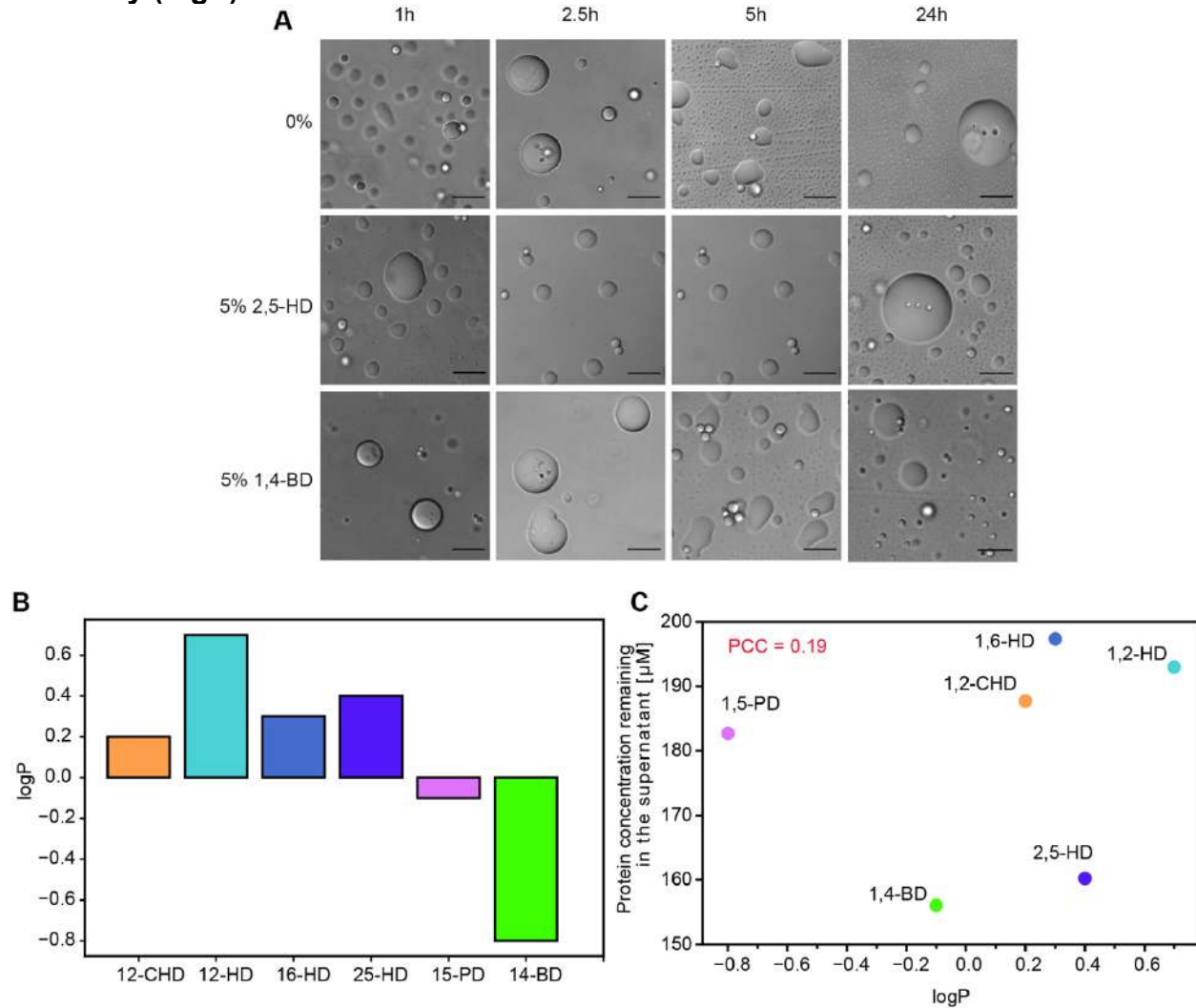
C



- ^1H temperature coefficients measured in 0% 1,6-hexanediol (magenta) and 5% (green). Dotted line represents the value for “average” solvation where lower solvation is above the line and higher solvation is below the line. Error bars represent standard error of the estimated slope using a linear regression algorithm.
- The difference in temperature coefficient, calculated by subtracting the values in 5% 1,6-HD from the values in 0% 1,6-HD.
- R^2 value of the linear fits used to extract the temperature coefficient from the set of 5 temperatures.

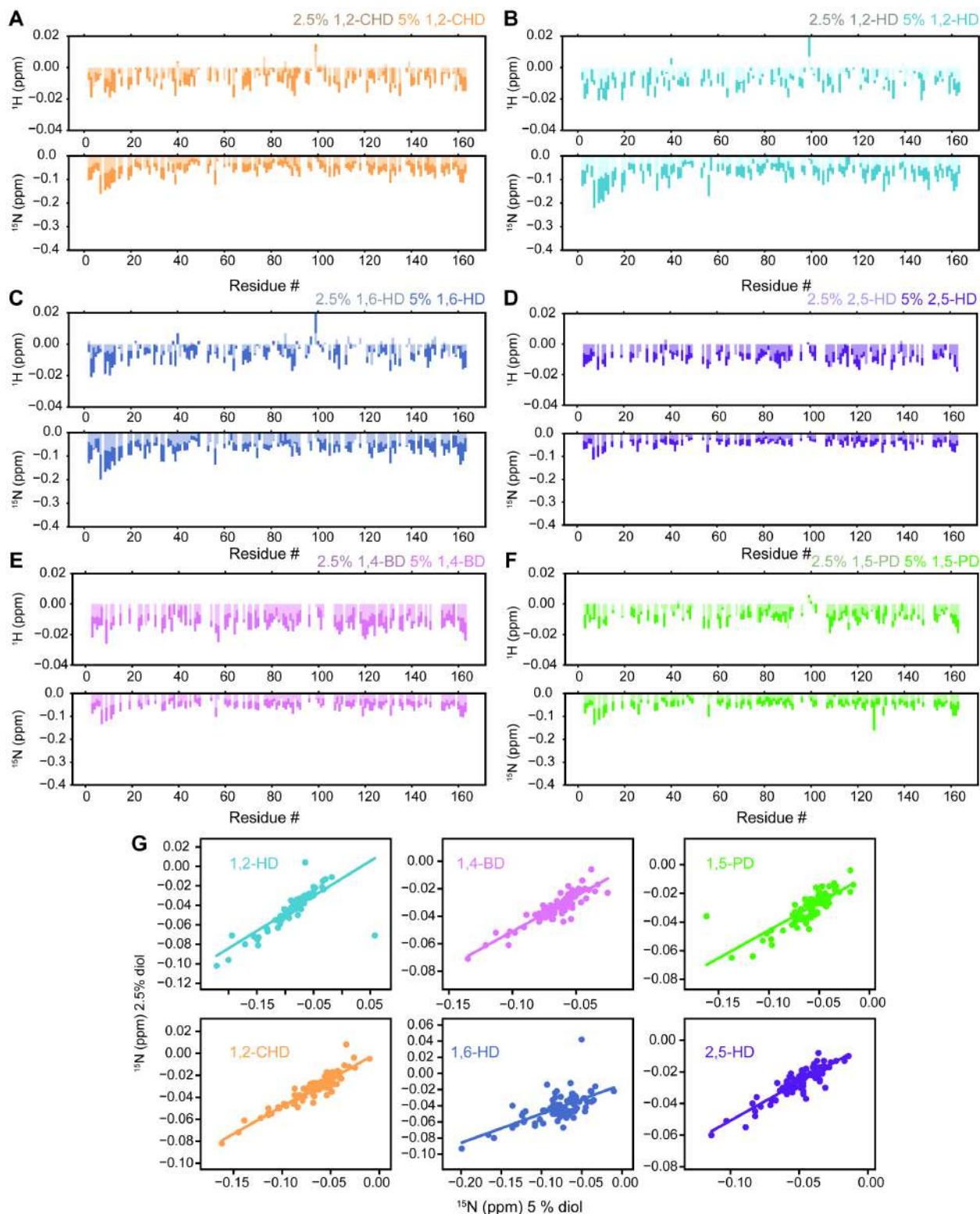
SI Figures

SI Figure 1: The effect on LLPS is not correlated with the predicted water solubility (logP) of each diol.



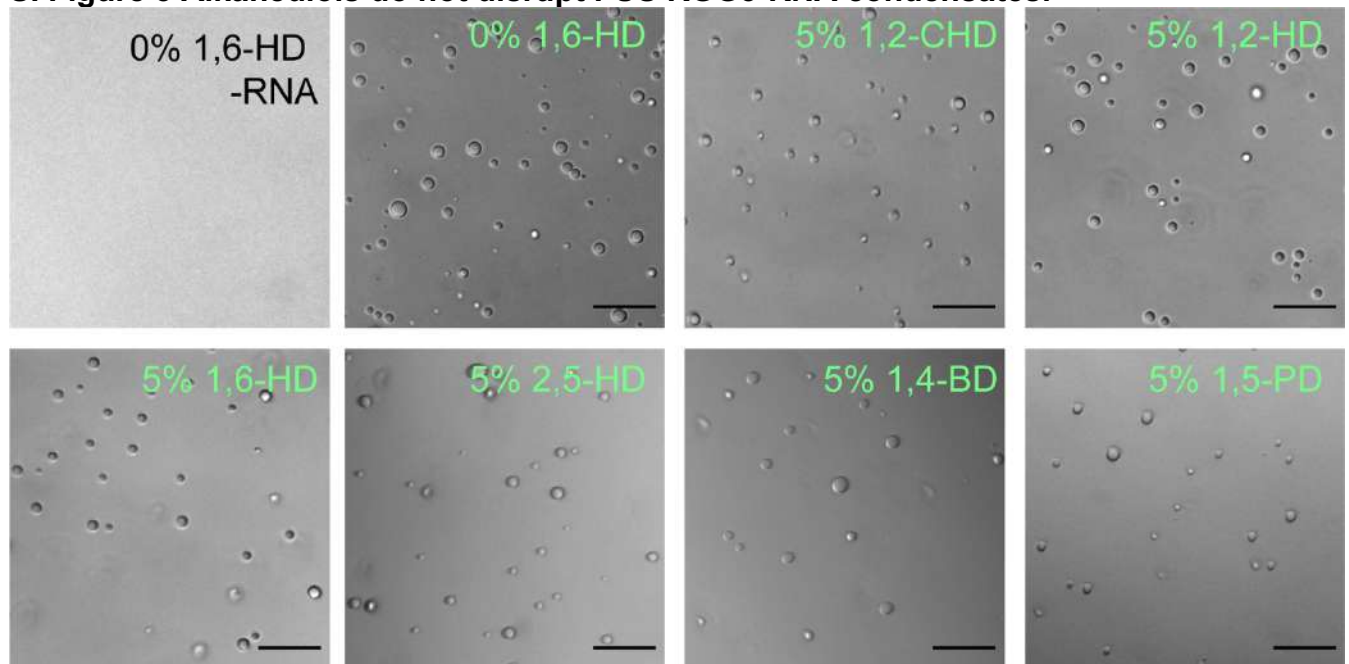
- FUS SYGQ LC droplets in the presence of 5% 2,5-hexanediol or 5% of 1,4-butanediol remain intact over time. 50 mM MES pH 5.5, 150 mM NaCl, 5% co-solvent, 200 μ M FUS SYGQ LC, Scale bars represent 50 μ m.
- Computationally predicted values of the octanol partition coefficient of each alkanediol. Log P corresponds to the logarithm of the ratio of the concentration of the solute in octanol versus in water.
- Correlation of logP presented in (b) versus protein remaining in the supernatant presented in Figure 1b shows that the effect of the alkanediols measured by the phase separation assay is not correlated with the hydrophobicity (as measured by the octanol log P) of the diols (PCC = 0.19).

SI Figure 2: Chemical shift perturbations of FUS SYGQ LC in the presence of different alkanediols.



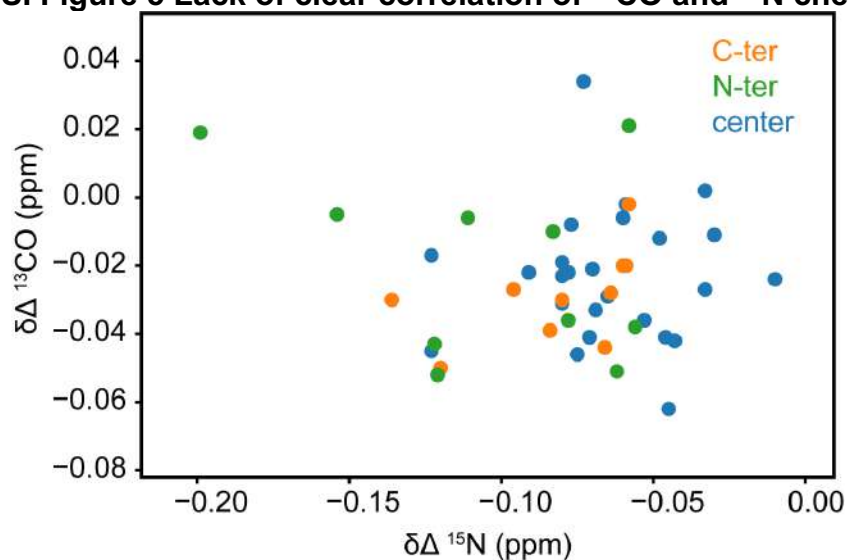
a-f) Chemical shift deviations for FUS SYGQ LC in the presence of different diols at 2.5% or 5% w/v in 50 mM MES pH 5.5, 150 mM NaCl
g) Correlation of ^{15}N chemical shift deviations for 2.5% and 5% diol.

SI Figure 3 Alkanediols do not disrupt FUS RGG3-RNA condensates.



Droplets were made in 50 mM MES pH 5.5, 150 mM NaCl, 5% co-solvent, 100 μ M FUS RGG3, 0.142 mg/ml polyadenylic acid (poly A) RNA and were imaged after 1 hour of incubation in room temperature. Scale bars represent 50 μ m.

SI Figure 5 Lack of clear correlation of ^{13}C O and ^{15}N chemical shifts



Backbone ^{13}C O and ^{15}N chemical shift perturbations due to addition of 5% 1,6 hexanediol are not markedly correlated in any region (N-terminal ten assigned residues, central (all other residues), or C-terminal ten assigned residues) of FUS SYGQ-rich LC.